Electronic Supplementary Information

Covalent organic framework spherical nanofibers bearing carbon quantum dots for boosting photocatalytic hydrogen production

Jiyuan Zang,[a] Yuting Zhao,[a] Lei Yu,[a] David J. Young,*[b] Zhi-Gang Ren[a] and Hong-Xi Li*[a]

[a]College of Chemistry, Chemical Engineering and Materials Science, Soochow University, Suzhou 215123, P. R. China. Email: lihx@suda.edu.cn

[b]James Watt School of Engineering, University of Glasgow, University Avenue, Glasgow, G12 8QQ UK. Email: David.J.Young@glasgow.ac.uk

EXPERIMENTAL SECTION

Materials. All chemicals used were of analytical grade or higher. Citric acid purchased from Macklin Inc. (Shanghai, China; purity greater than 99.5%). 2,4,6-tris(4-aminophenyl)-1,3,5-triazine purchased from Aladdin Chemistry Co. Ltd. (Shanghai, China; purity greater than 95%). 2,4,6-trihydroxybenzene-1,3,5-tricarbaldehyde purchased from Adamas-beta (Shanghai, China; purity greater than 98%).

Synthesis of CQDs. Citric acid (5 mmol) and ethylenediamine (335 μL) were dissolved in 10 mL of deionized water. The mixed solution was added to a 25 mL Teflon Lin autoclave and heated at 200 °C for 5 h. After cooling to room temperature, the reaction mixture was subjected to dialysis for 24 h. After cooling to room temperature, this reaction solution was freeze-dried for 48 h to obtain solid CQDs.

Synthesis of TAPT-COF. To a Pyrex glass tube (50 mL) was added 2,4,6-trihydroxybenzene-1,3,5-tricarbaldehyde (TFP; 84 mg 0.4 mmol), 2,4,6-tris(4-aminophenyl)-1,3,5-triazine (TAPT; 141.2 mg, 0.4 mmol), mesitylene (3 mL), and 1,4-dioxane (3 mL). The mixture was ultrasonicated for 20 min and acetic acid (6 M, 0.6 mL) was added with a syringe. The glass tube was flash frozen in a N_2 liquid bath and degassed by three freeze-pump-thaw cycles and then then sealed. After standing at ambient temperature for 2 hours, the mixture was stirred at 120 °C for 3 days. The resulting orange precipitate was collected by centrifugation, and then washed with N,N-dimethylformamide, tetrahydrofuran and ethanol. The solids were then dried under vacuum at 80 ℃ for 24 h.

Synthesis of TAPT-COF-CQDs-X. TAPT-COF-CQDs-X (X = 1, 2, 3, 4, 5 mg) were prepared in a similar manner to that used for the preparation of TAPT-COF, but using CQDs (1, or 2, 3, 4, 5 mg), TFP (84 mg, 0.4 mmol), and TAPT (141.2 mg, 0.4 mmol) as starting materials.

Synthesis of TAPT-COF/CQDs-3%. A certain weight ratio of TAPT-COF to CQDs was mixed in ethanol (10 mL). The suspension was ultrasonicated for 2 h and dry at 80 °C. TAPT-COF/CQDs-3% is a sample with a weight percentage of 3 wt% of CQDs relative to TAPT-COF.

Photocatalytic H_2 evolution. To a quartz flask (200 mL) was added photocatalyst (10 mg), triethanolamine (TEOA; 5 mL), distilled water (50 mL), and Pt (3 wt% from 2.0 mg H_2PtCl_6). The mixture was sonicated for 30 min, then evacuated and flushed with nitrogen three times, and linked to a glass automatic on-line trace gas analysis system (Labsolar-6A, Beijing Perfect Light Technology Co., Ltd, China). The reaction was irradiated with a xenon lamp (300 W) with cutoff wavelengths of 420 nm or 520 nm, and maintained at 25 ℃ by water cooling. The amount of evolved H_2 was periodically measured using online gas chromatography (GC7900, Tianmei, China) with N_2 as the carrier gas.

Photoelectrochemical characterization. Electrochemical impedance spectroscopy (EIS) and transient photocurrent measurements were obtained on an electrochemical analyzer (CHI760E Instruments) with a conventional three-electrode cell with Pt wire as the counter electrode, Ag/AgCl as a reference electrode and 0.1 mol L^{-1} Na_2SO_4 as the electrolyte. The working electrode was prepared by spreading TAPT-COF-CQDs-

X (1 mg mL^{-1} in isopropanol with 32 μL 5 wt% Nafion) on F-doped tin oxide glass. The light source was a xenon lamp (300 W) with a 420 nm or 520 nm cutoff filter.

Apparent quantum efficiency (AQE) measurements. AQE for H_2 evolution was measured under the illumination of a xenon lamp (300 W) with different bandpass filters of 420 ± 10 nm, 440 ± 10 nm, 460 ± 10 nm, and 520 ± 10 nm with intensities of 2.25, 2.97, 2.60 and 3.47 $mW \cdot m^{-2}$, respectively. Pure TAPT-COF or TAPT-COF-CQDs-3 was suspended in H_2O (50 mL) with TEOA (5 mL) and H_2PtCl_6 (2.0 mg). The irradiation area was confined to 3.14 × 3 cm^2. The value of AQE was calculated according to the following equation:

$$\eta_{AQE} = \frac{N_e}{N_p} \times 100\%$$

$$= \frac{2 \times \eta \times N_A}{\frac{E_{total}}{E_{photon}}} \times 100\%$$

$$E_{total} = S \times P \times t$$

$$E_{photon} = h \times \frac{c}{\lambda}$$

$$\eta_{AQE} = \frac{2 \times n \times N_A \times h \times c}{S \times P \times t \times \lambda} \times 100\%$$

where N_e is the number of generated electrons for H_2, N_p is the number of incident photons, n is the molar mass of H_2 molecules produced over 1 hour, λ is the wavelength of the monochromatic light (4.20×10^{-7}, 4.40×10^{-7}, 4.60×10^{-7}, or 5.20×10^{-7}m), S (the irradiation area) = 3.8×10^{-3} m^2, P is the intensity of irradiation light ($W \cdot m^{-2}$), N_A (Avogadro constant) = 6.022×10^{23} mol^{-1}, h (the Planck's constant) = 6.626×10^{-34} J·s, c (the light speed) = 3×10^8 $m \cdot s^{-1}$, t (the photoreaction time) = 3600 s.

The adsorption free energy of a H atom. The adsorption free energy for a H atom on a substrate was calculated using the model of Nørskov et al.:

$$\Delta G_H = \Delta E_H + \Delta E_{ZPE} - T\Delta S$$

where ΔE_{ZPE} and ΔS are the changes of zero-point energy and entropy, T is the absolute temperature. $\Delta E_{ZPE} - T\Delta S \approx 0.26$ eV is generally used for HER. ΔE_H denotes the adsorption energy of a hydrogen atom on a substrate and was calculated by:

$$\Delta E_H = E(sub/H) - E(sub) - E(H_2)/2$$

where E(sub/H), E(sub) and $E(H_2)$ are the total energies of a H atom on a substrate, substrate alone and hydrogen gas, respectively.

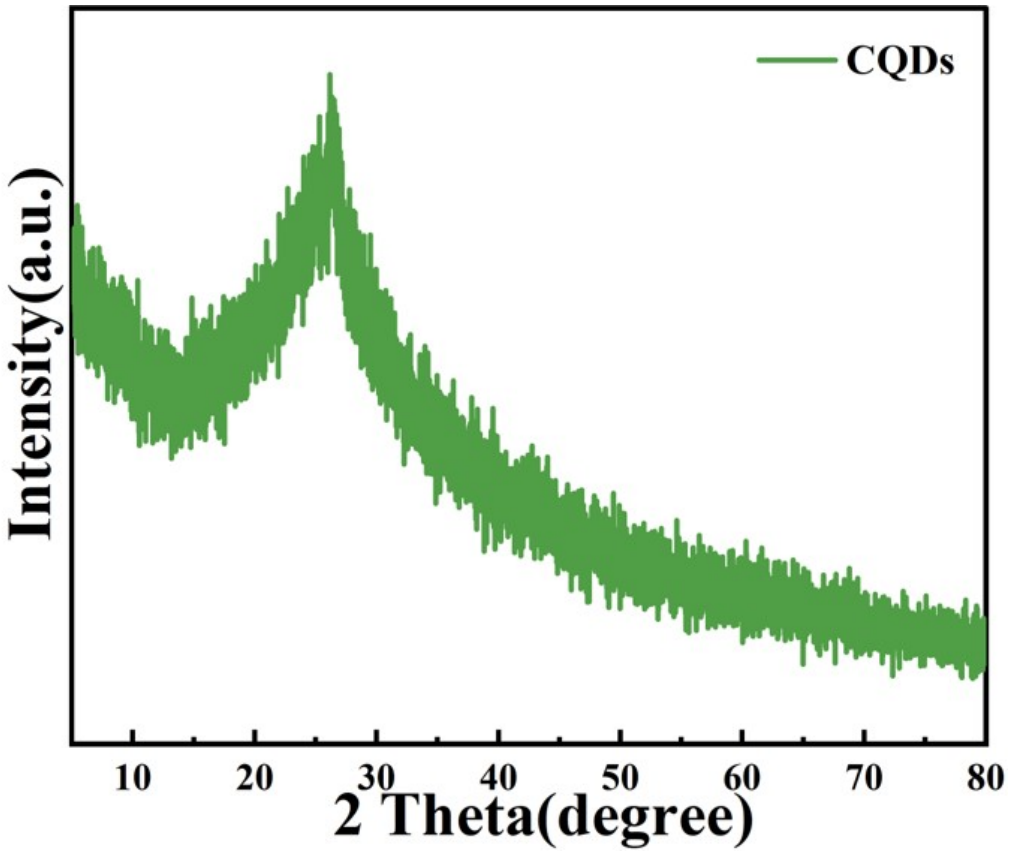

Fig. S1 PXRD patterns of CQDs.

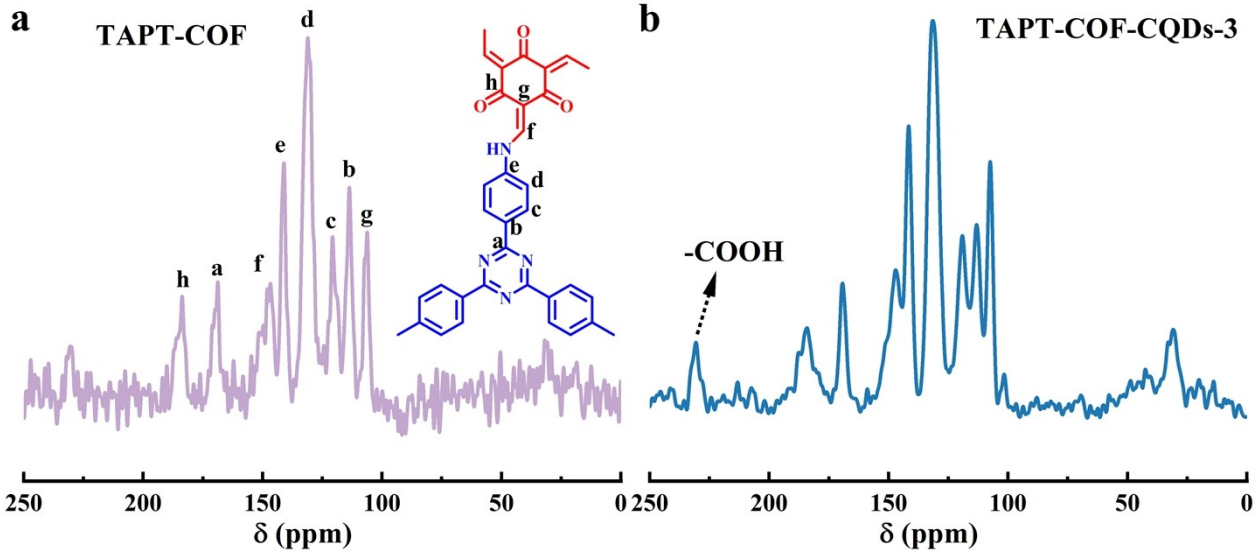

Fig. S2 Solid-state ^{13}C NMR Spectra of TAPT-COF (a) and TAPT-COF-CQDs-3 (b).

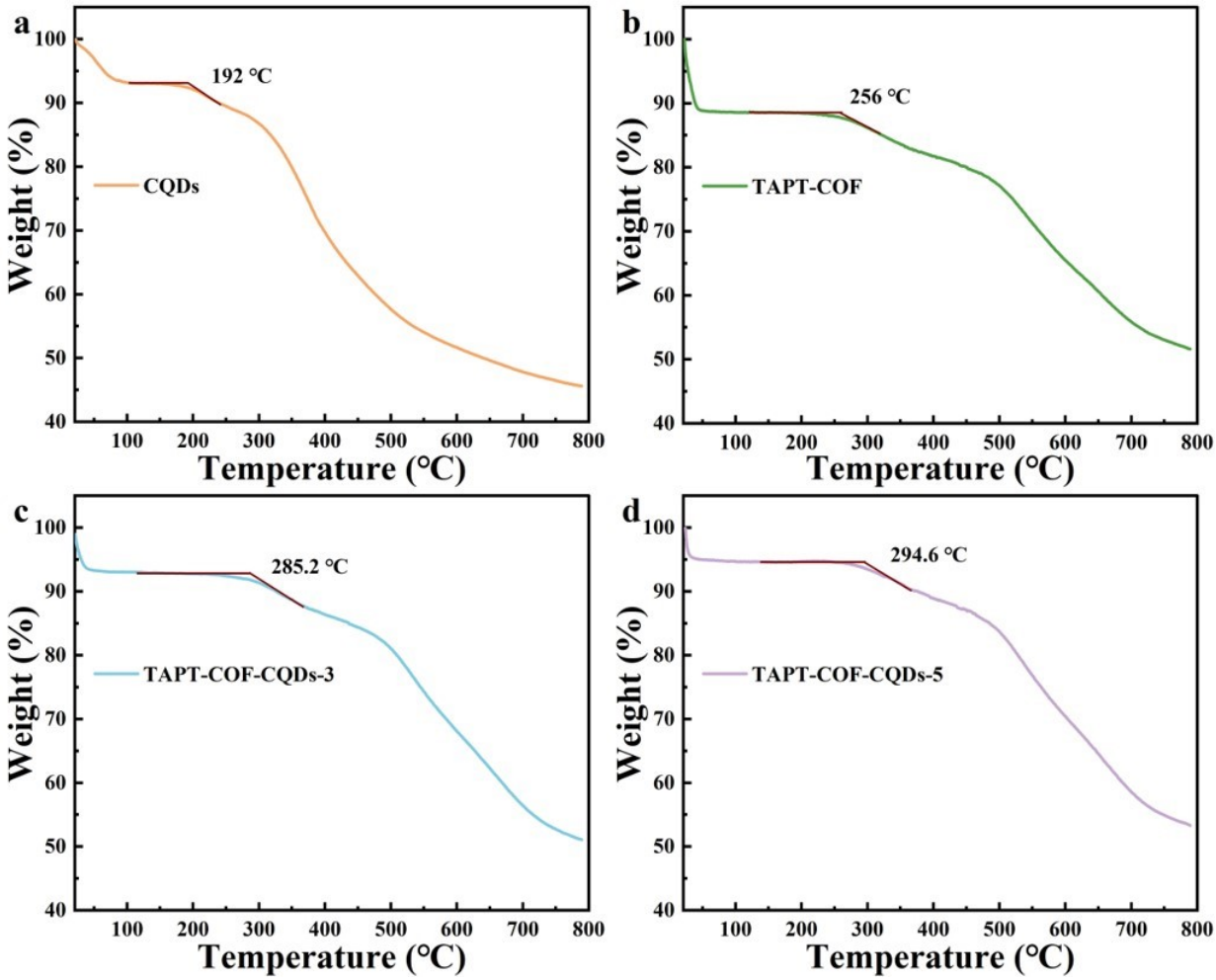

Fig. S3 TGA curves of (a) CQDs, (b) TAPT-COF, (c) TAPT-COF-CQDs-3, (d) TAPT-COF-CQDs-5.

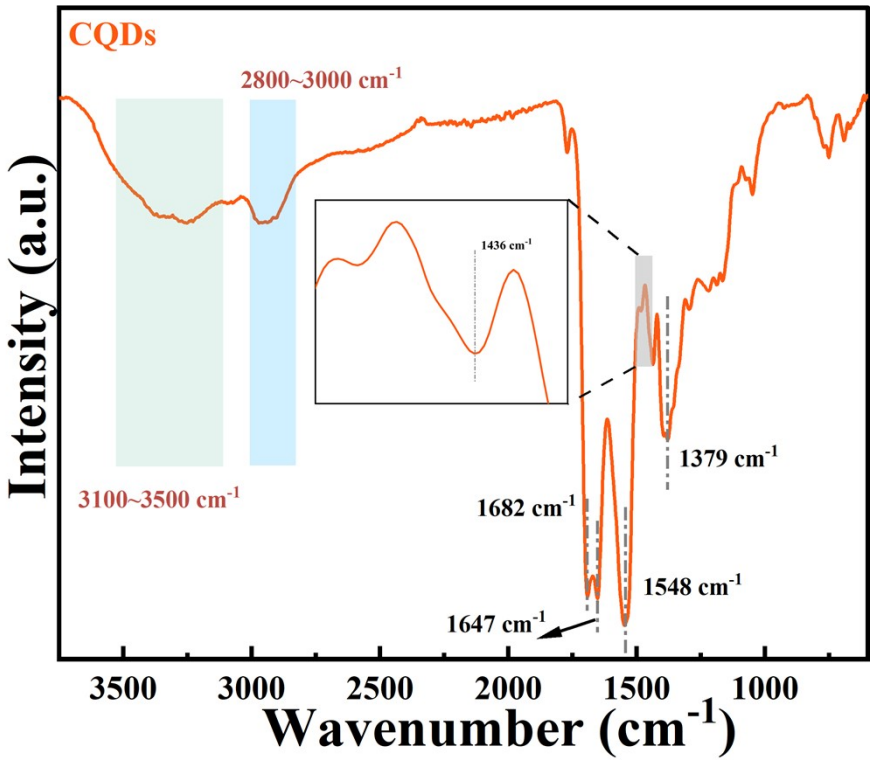

Fig. S4 FT-IR spectra of CQDs.

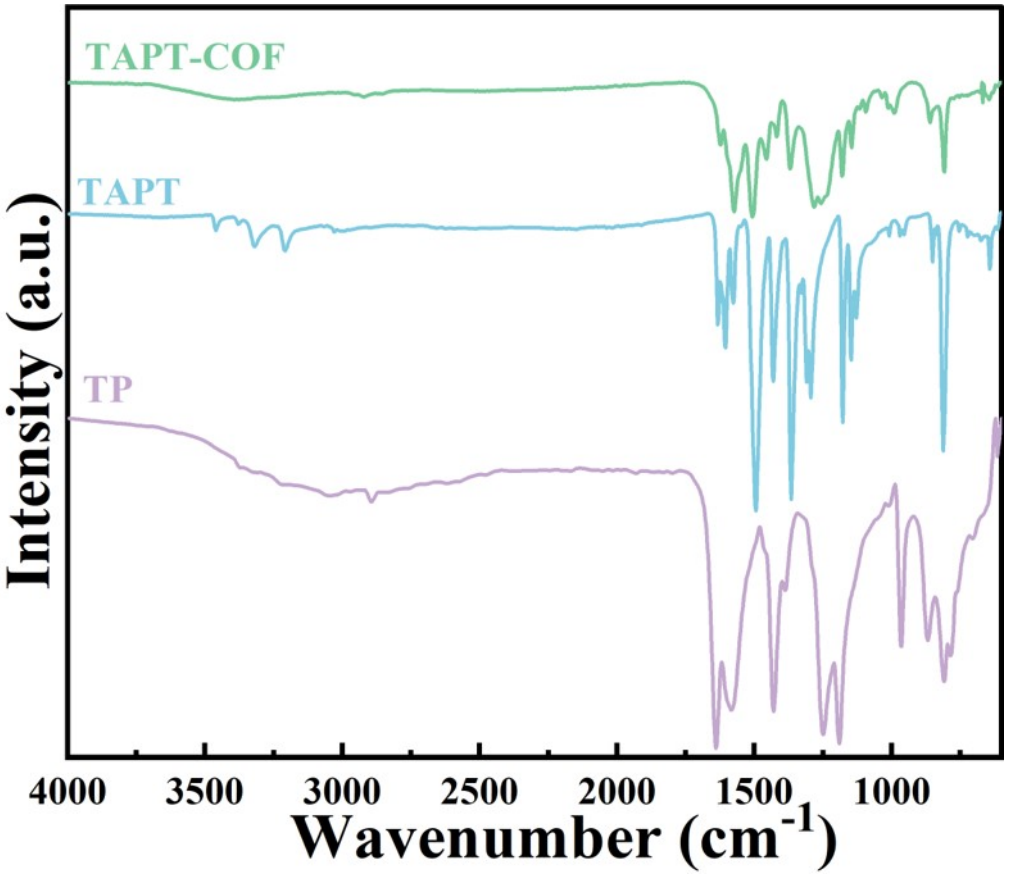

Fig. S5 FT-IR spectra of TAPT, TFP and TAPT-COF.

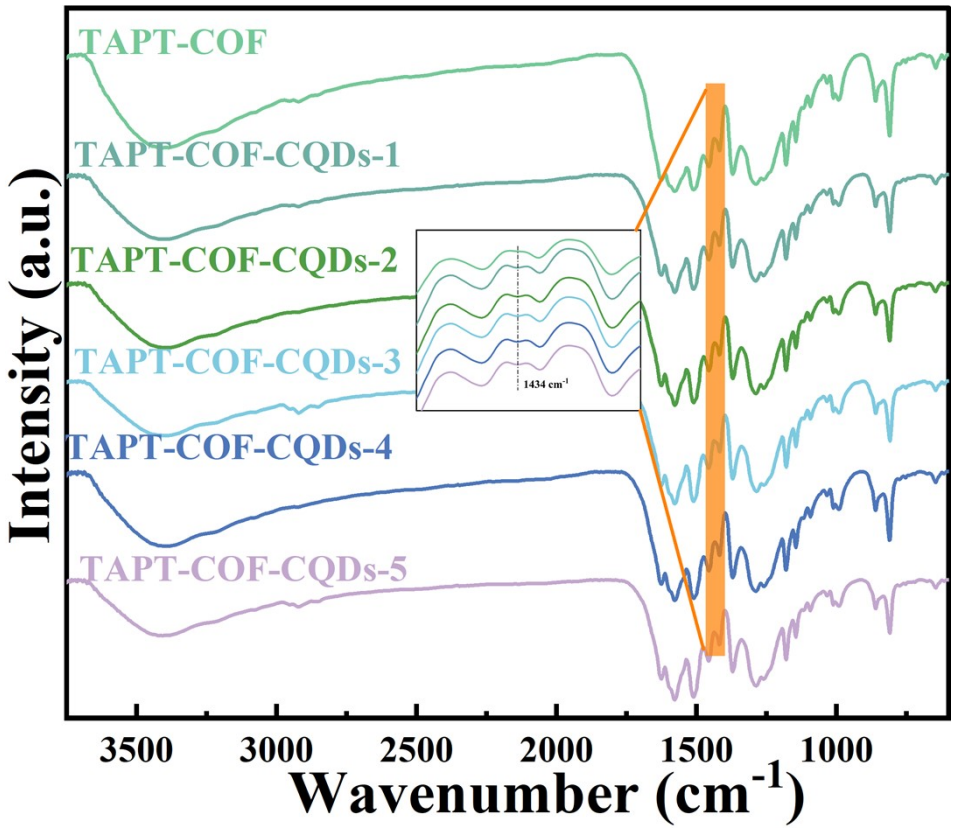

Fig. S6 FT-IR spectra of TAPT-COF-CQDs-X (X = 0, 1, 2, 3, 4, 5).

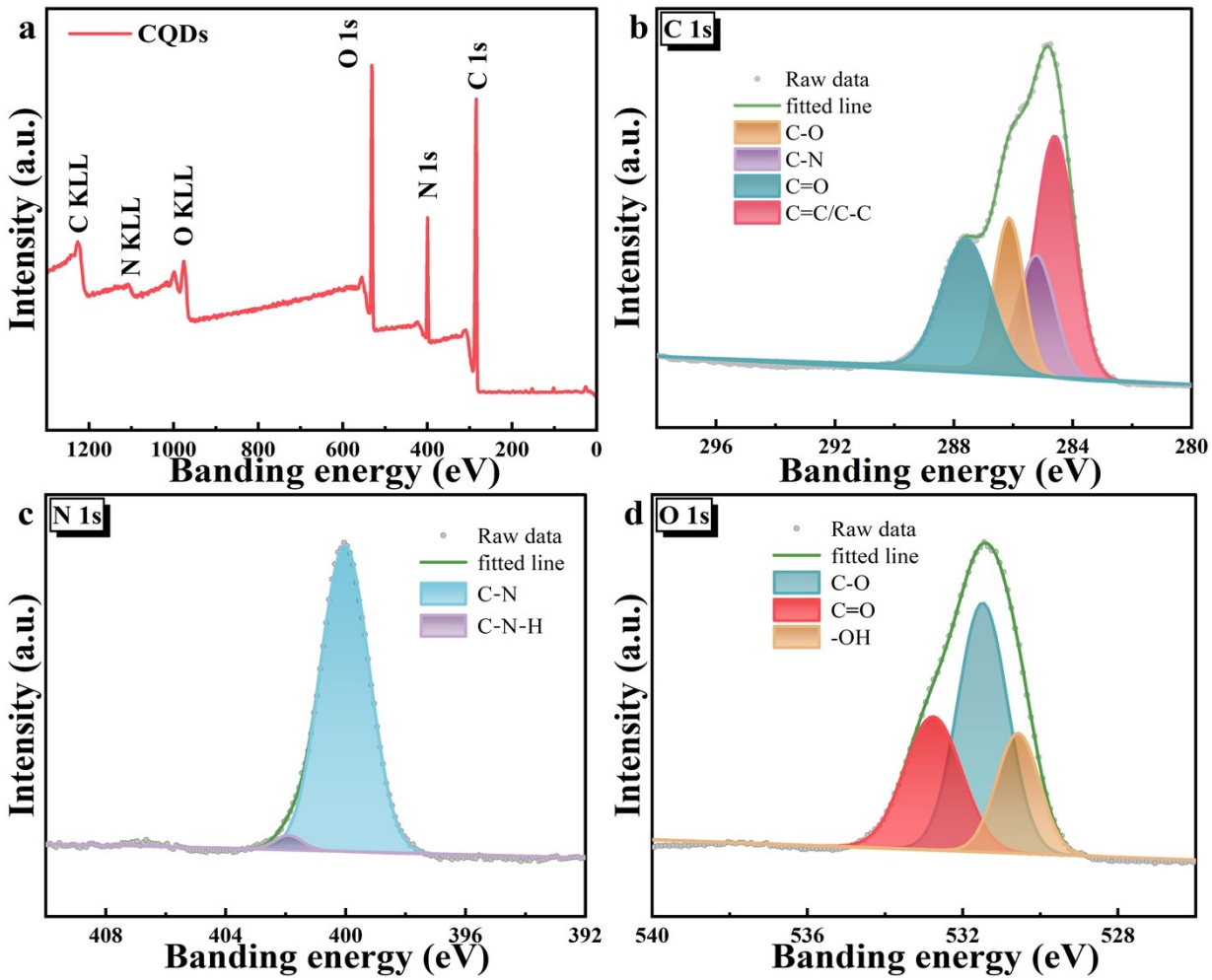

Fig. S7 (a) XPS survey spectra of CQDs. High-resolution XPS spectra of (b) C 1s and (c) O 1s and (d) N 1s of CQDs.

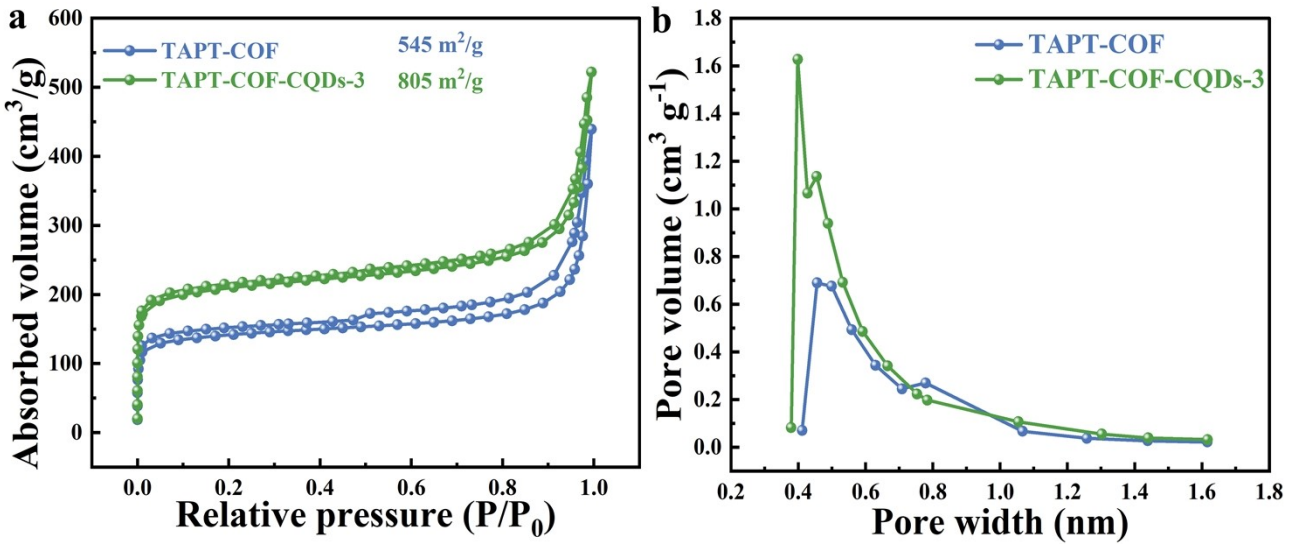

Fig. S8 N_2 adsorption–desorption isotherm (a) and pore size distribution (b) of TAPT-COF and TAPT-COF-CQDs-3.

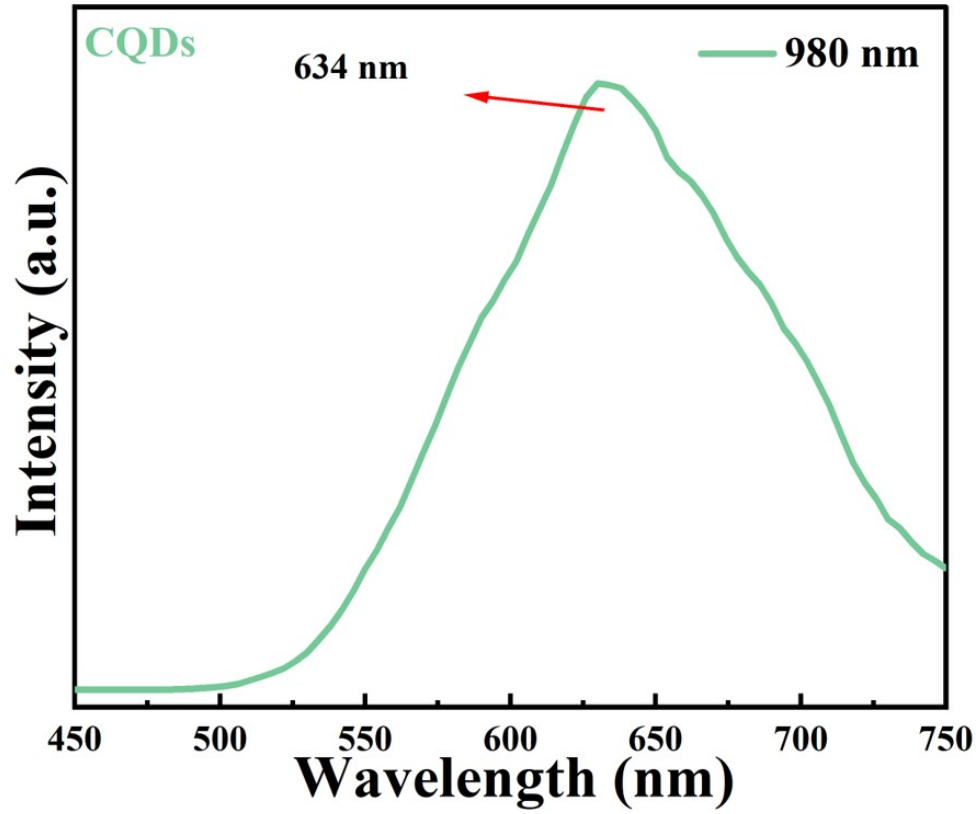

Fig. S9 Up-converted PL spectra of CQDs.

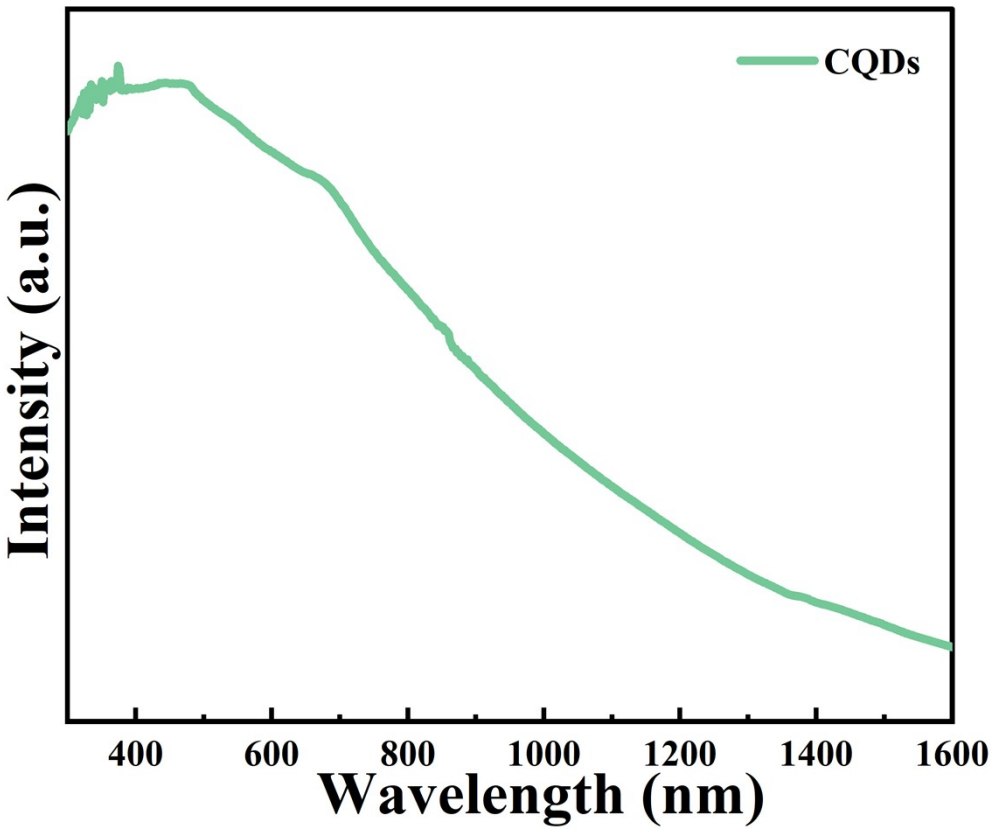

Fig. S10 UV-vis diffuse reflectance spectra (UV-DRS) of CQDs.

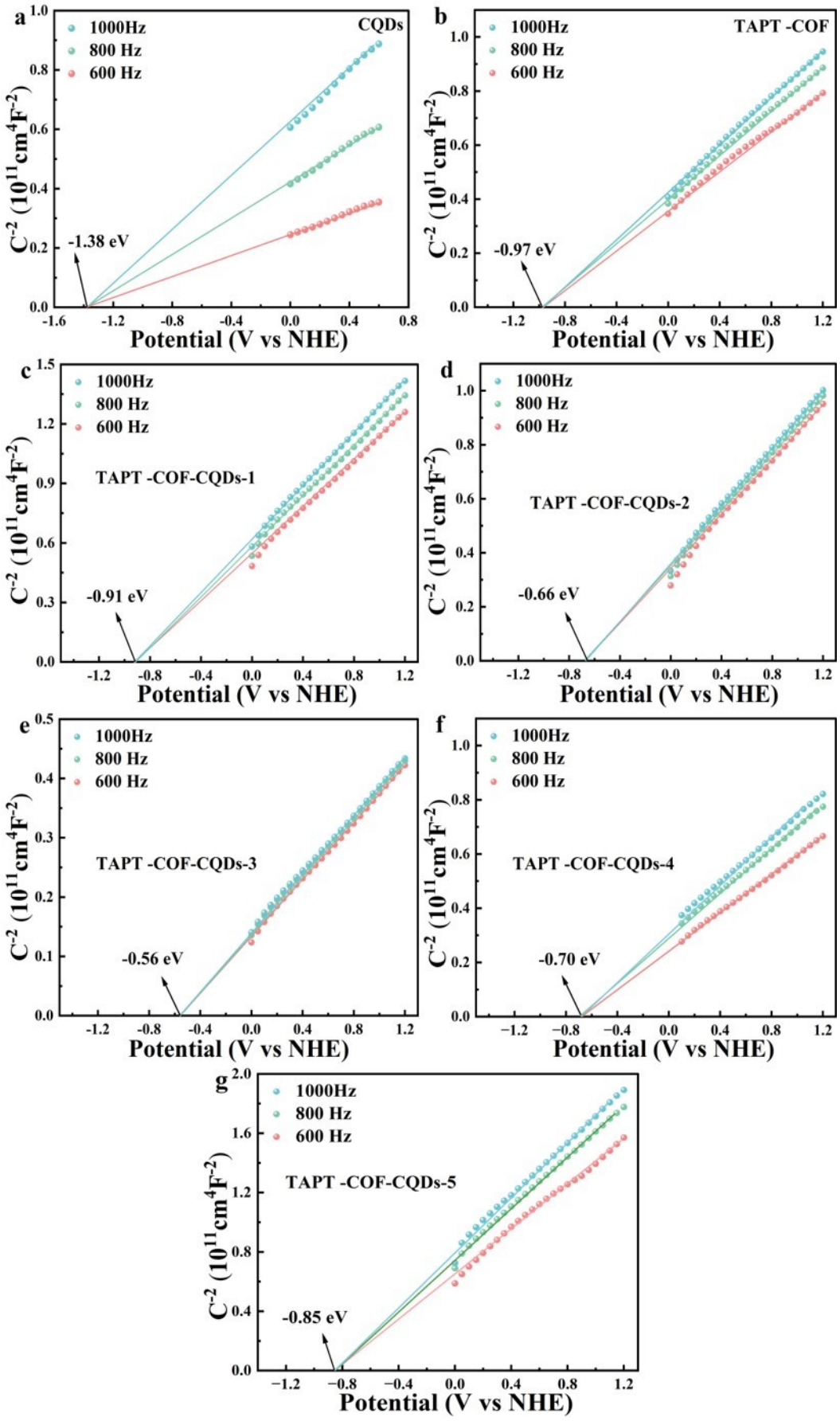

Fig. S11 Mott-Schottky plots of CQDs and TAPT-COF-CQDs-X (X=0, 1, 2, 3, 4, 5).

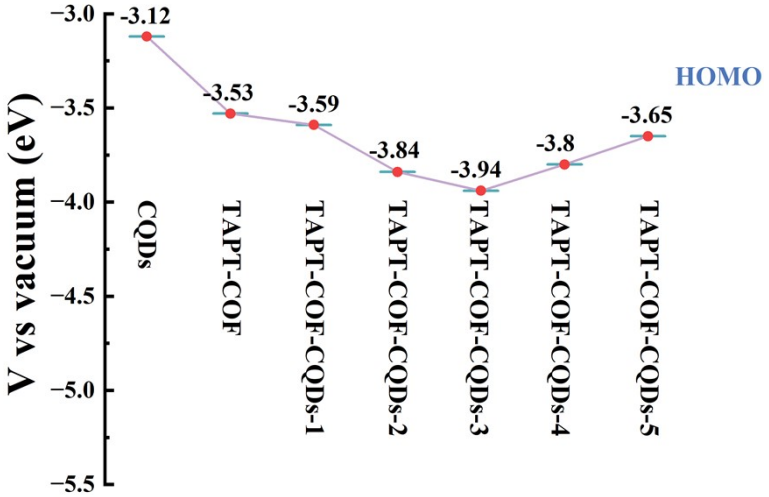

Fig. S12 HOMO positions of the photocatalysts.

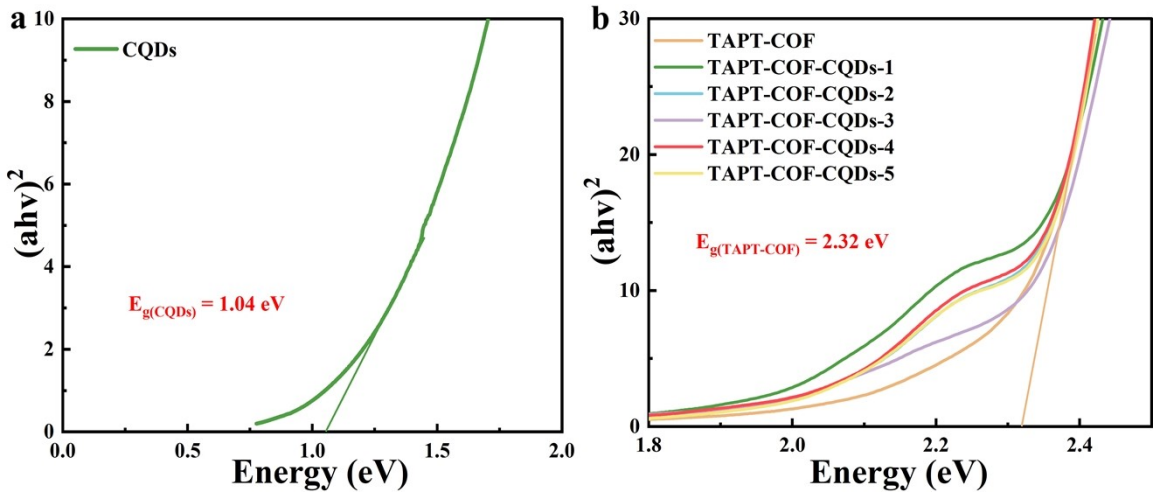

Fig. S13 Tauc plots of CQDs (a) and TAPT-COF-CQDs-X (X=0, 1, 2, 3, 4, 5) (b).

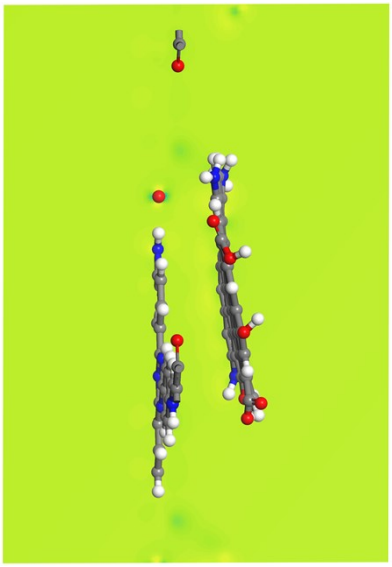

Fig. S14 The electron localization function (including cut) of TAPT-COF-CQDs.

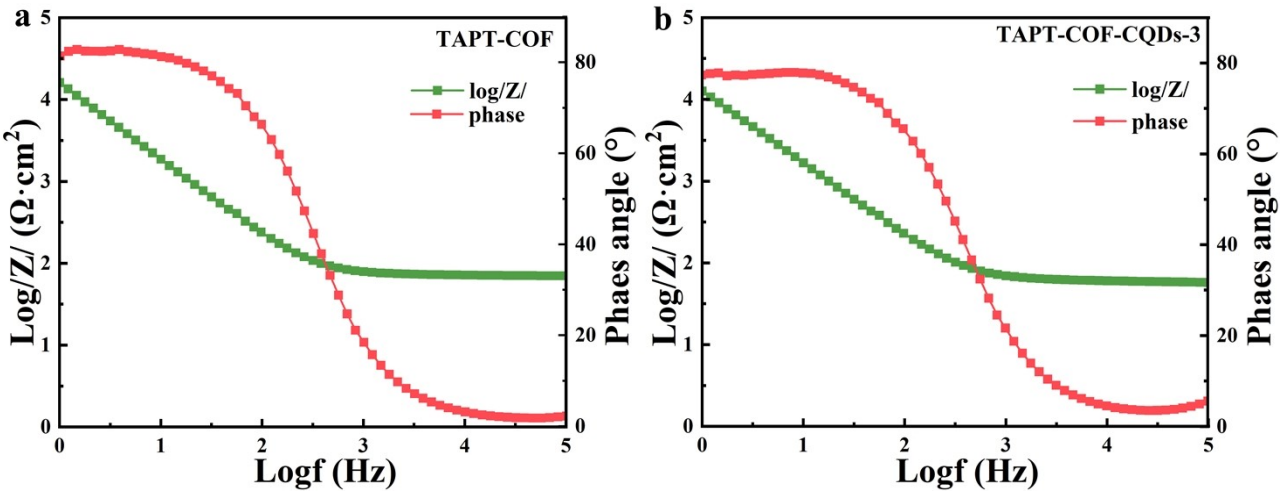

Fig. S15 The Bode plots of TAPT-COF (a) and TAPT-COF-CQDs (b).

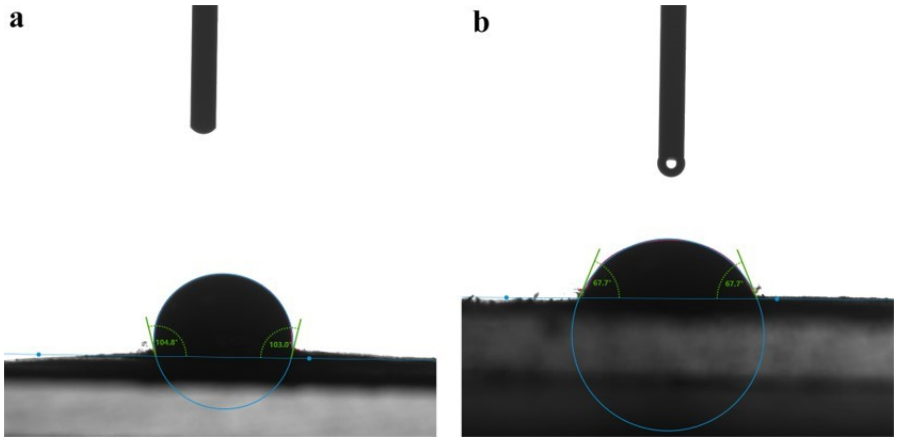

Fig. S16 Water contact angle measurements of (a) TAPT-COF and (b) TAPT-COF-CQDs-3.

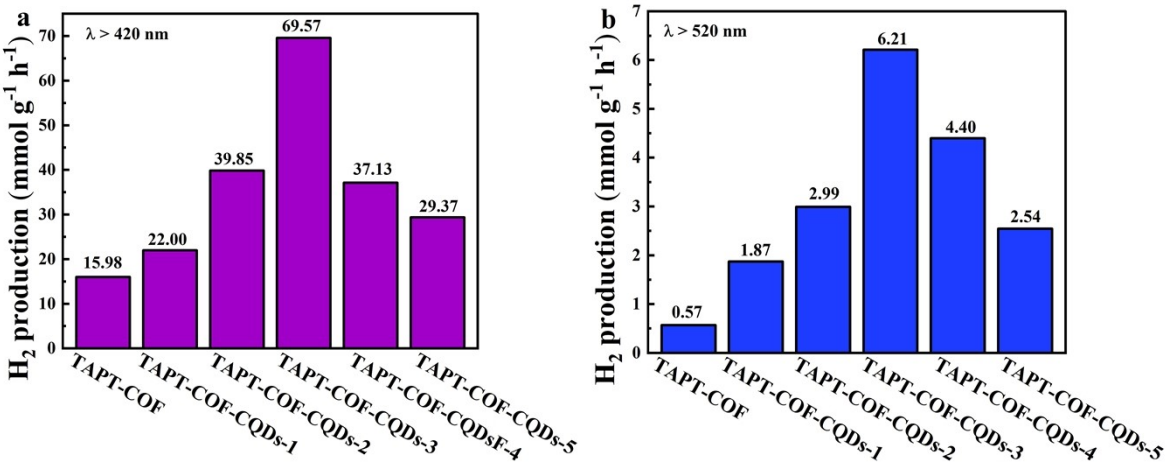

Fig. S17 Hydrogen production performance under (a) $\lambda \geq 420$ nm (b) $\lambda \geq 520$ nm.

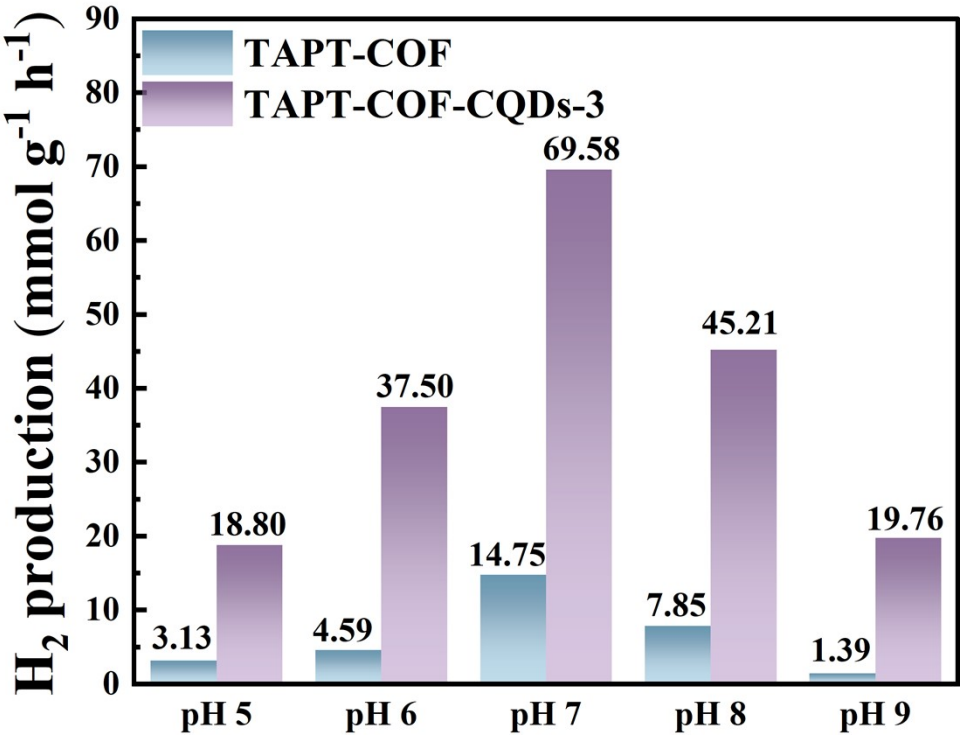

Fig. S18 Hydrogen production performance for TAPT-COF and TAPT-COF-3 at different pH.

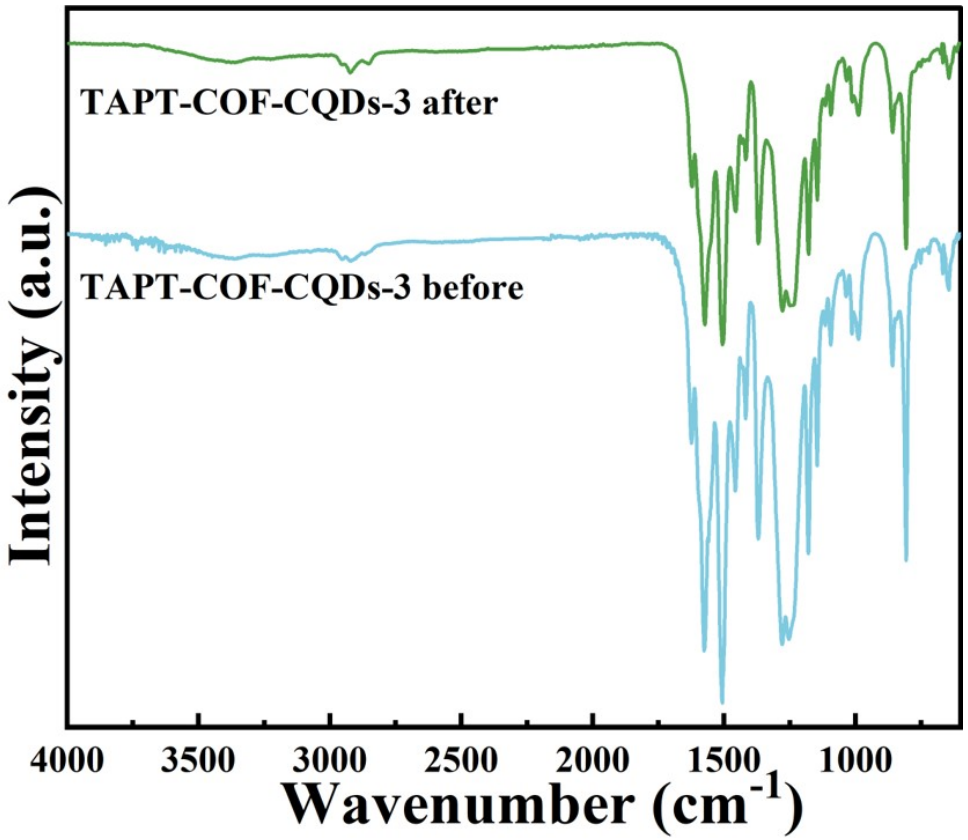

Fig. S19 FT-IR spectra of TAPT-COF-CQDs-3 before and after photocatalysis.

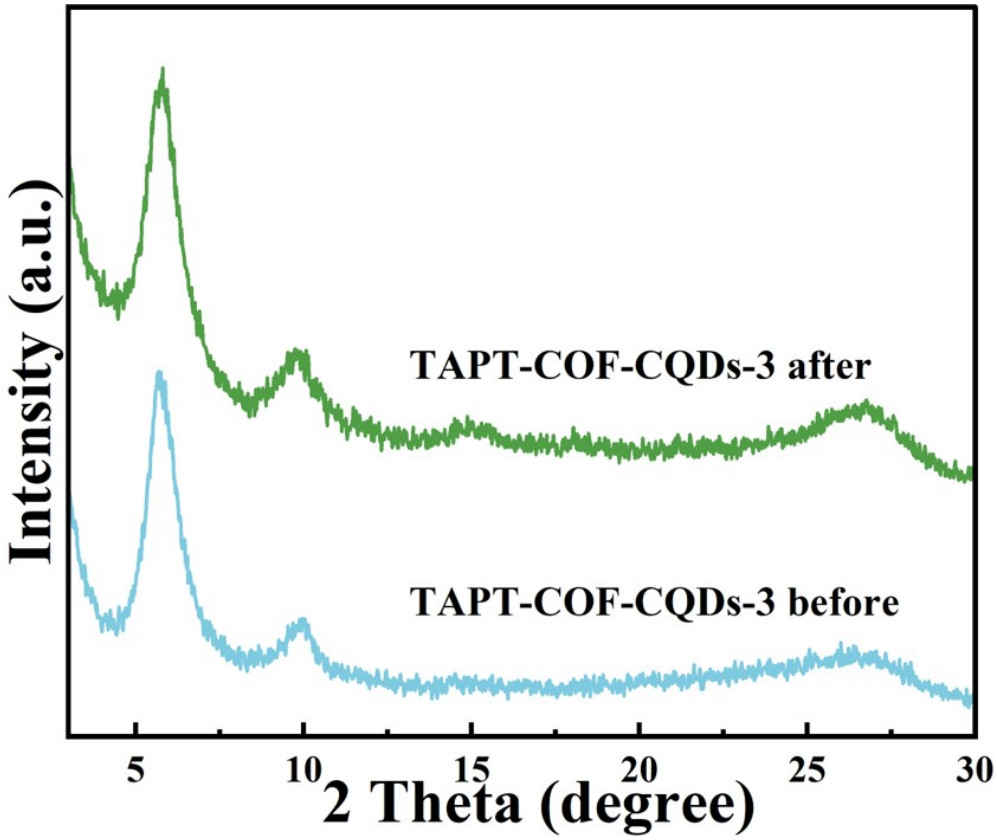

Fig. S20 PXRD patterns of TAPT-COF-CQDs-3 before and after photocatalysis.

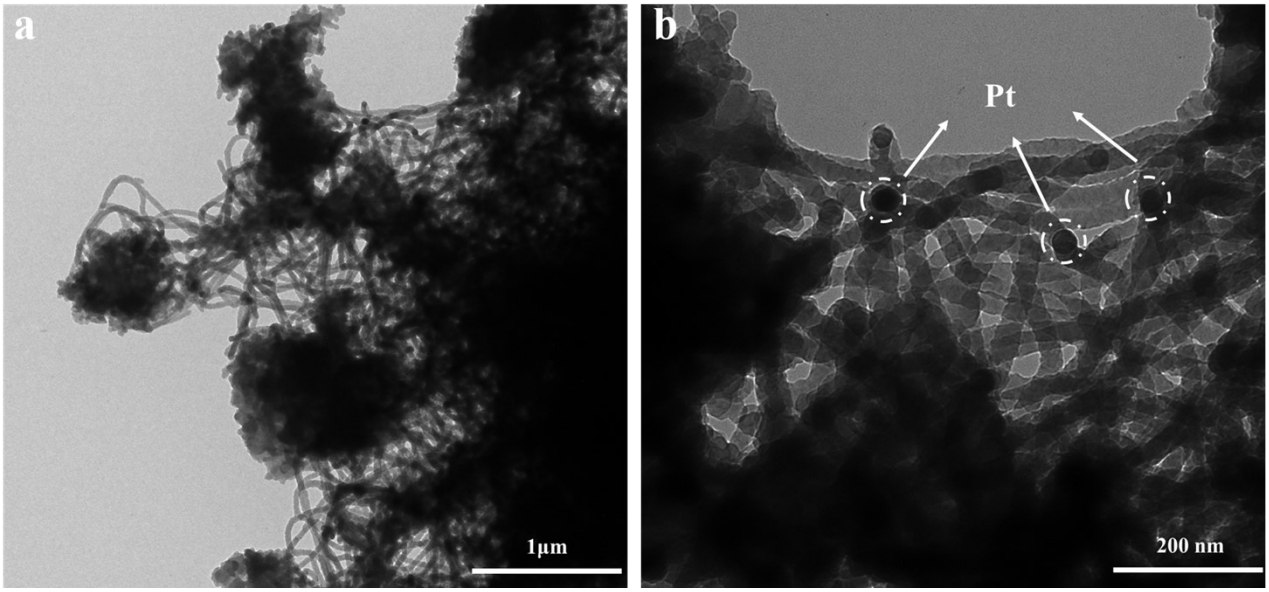

Fig. S21 TEM of TAPT-COF-CQDs-3 before photocatalysis.

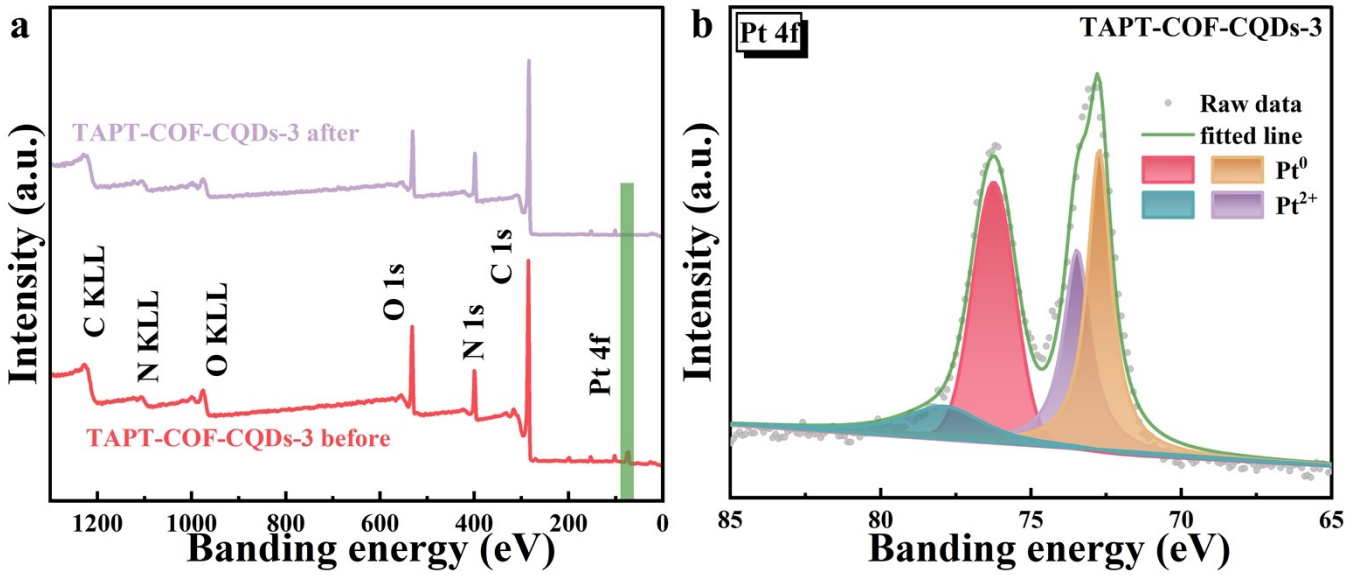

Fig. S22 Full XPS spectra (a) and high-resolution Pt 4f XPS spectra (b) of TAPT-COF-CQDs-3 after the photocatalytic reaction.

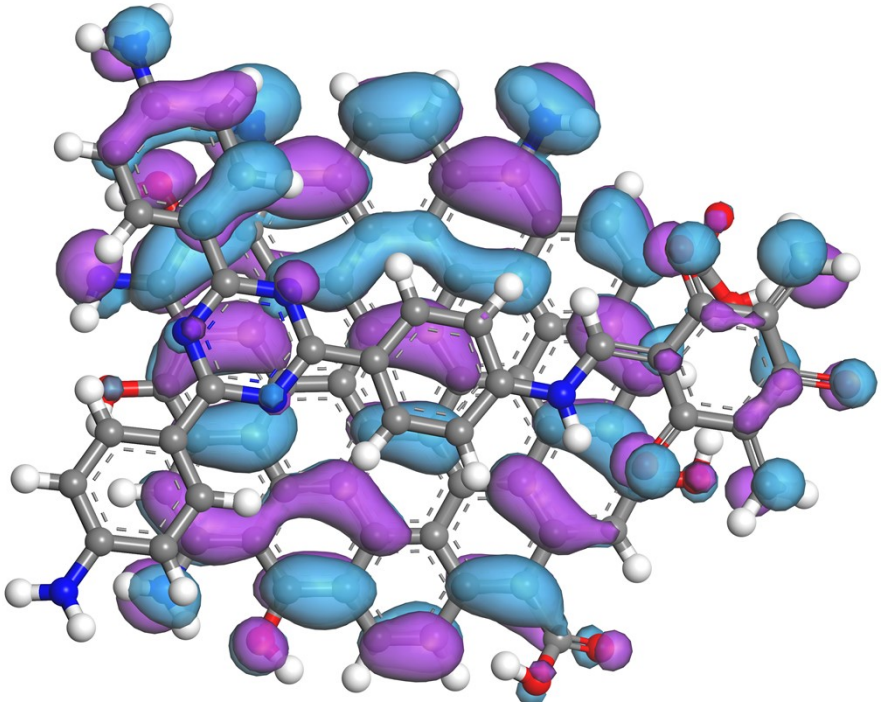

Fig. S23 HOMO of TAPT-COF-CQDs (001) heterojunction from the top view.

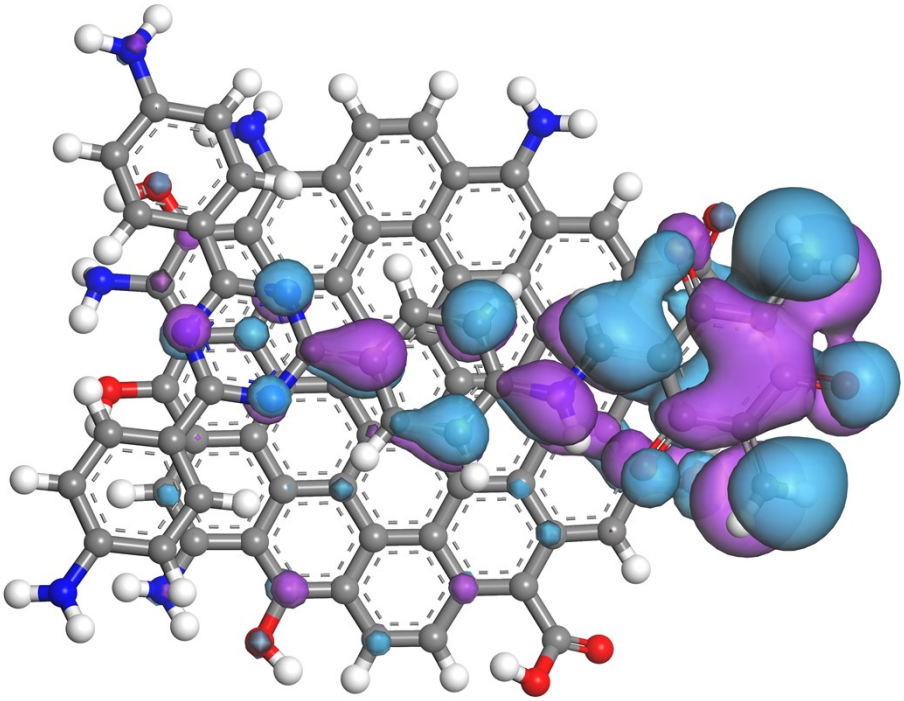

Fig. S24 LUMO of TAPT-COF-CQDs (001) heterojunction from the top view.

Table:

Table S1 The peak position, area, and proportion of C 1s in XPS of TAPT-COF and TAPT-COF-CQDs-3.

		C=O	C=N	C-N	C=C
TAPT-COF	Location	289.2	286.4	285.5	284.6
	Area	13940	19599	2040	36319
	Ratio	19.39%	27.26%	2.84%	50.51%
TAPT-COF-CQDs-3	Location	289.6	286.4	285.1	284.6
	Area	13494	19490	6727	30846
	Ratio	19.12%	27.62%	9.53%	43.72%

Table S2 The peak position, area, and proportion of N 1s in XPS of TAPT-COF and TAPT-COF-CQDs-3.

		C-N-H	C-N	C=N
TAPT-COF	Location	402.33	400.08	398.58
	Area	2356	8703	7055
	Ratio	13.01%	48.05%	38.95%
TAPT-COF-CQDs-3	Location	404.8	400.1	398.6
	Area	1399	11689	7046
	Ratio	6.95%	58.06%	35.00%

Table S3 The peak position, area, and proportion of O 1s in XPS of TAPT-COF and TAPT-COF-CQDs-3.

		-OH	C-O	C=O
TAPT-COF	Location	533.5	531.7	530.6
	Area	5058	15752	4757
	Ratio	19.88%	61.54%	18.58%
TAPT-COF-CQDs-3	Location	533.3	531.97	530.88
	Area	6642	7551	10572
	Ratio	26.82%	30.49%	42.69%

Table S4 Fluorescence lifetime decay obtained by exciting TAPT-COF and TAPT-COF-CQDs-3 with a $\lambda_{ex} = 375$ nm laser.

	B_1	τ_1/ns	B_2	τ_2/ns	B_3	τ_3/ns	τ_{avg}/ns
TAPT-COF	9756.092	0.995	1835.421	0.995	1903.4376	3.072	1.69
TAPT-COF-CQDs-3	6181.251	0.851	9252.845	0.851	1048.790	3.020	1.27

Table S5 Comparison of photocatalytic HER performances of reported composite porous materials.

Photocatalyst	Sacrificial	Co-catalyst	Light (nm)	Activity ($\mu mol\ g^{-1}\ h^{-1}$)	Ref.
TAPT-COF-CQDs-3	TEOA	Pt	420	69512	This work
CN/TMP	TEOA	Pt	200	2057	S1
NH_2–MIL@SNW-1	TEOA	Pt	420	1949	S2
In_2O_3/BDA-DHTA-COF	AA	Pt	420	9691	S3
CTF-1/rGO-2	TEOA	Pt	420	894	S4
$C_{0.24}$/CTF-1	TEOA	Pt	400	2240	S5
COF/CN	AA	Pt	380	27540	S6
CdS/COF	AA	Pt	420	15100	S7
CTF@Au@TiO_2	TEOA	Au, Chloroplatinic acid	420	4288	S8
Tz-TA/g-C_3N_4	TEOA	Pt	420	5426	S9
MOF/COF	TEOA	Pt	420	360	S10
AA = ascorbic acid; TEOA = triethanolamine.					

References：

S1. L. Wang, R. Lian, Y. Zhang, X. Ma, J. Huang, H. She, C. Liu and Q. Wang, *Appl. Catal. B: Environ.*, 2022, **315**, 121568.

S2. Y. Wan, H. Yang, Q. Shang, Q. Cheng, H. Zhou and Z. Pan, *Environ. Sci-Nano*, 2022, **9**, 3081-3093.

S3. J. Yi, L. Zhang, W. Wang, Q. Yi, H. Wu, J. Li and J. Guo, *Fuel*, 2024, **355**, 129470.

S4. Z. Tan, P. Zhang, Q. Chen, S. Fang, G. Huang, J. Bi and L. Wu, *Catal. Sci. Technol.*, 2021, **11**, 1874-1880.

S5. Y. Chen, G. Huang, Y. Gao, Q. Chen and J. Bi, *Int. J. Hydrogen Energ.*, 2022, **47**, 8739-8748.

S6. A. E. Hassan, A. M. Elewa, M. S. A. Hussien, A. F. M. El-Mahdy, I. M. A. Mekhemer, I. S. Yahia, T. A. Mohamed, H. H. Chou and Z. Wen, *J. Colloid Interf. Sci.*, 2024, **653**, 1650-1661.

S7. G. Sun, J. Zhang, B. Cheng, H. Yu, J. Yu and J. Xu, *Chem. Eng. J.*, 2023, **476**, 146818.

S8. X. Han, Y. Dong, J. Zhao, S. Ming and Y. Xie, *Int. J. Hydrogen Energ.*, 2022, **47**, 18334-18346.

S9. M. Liu, F. Zhao, Y. Chu, J. Zhao, F. Meng and Y. Han, *Chem. Eng. Sci.*, 2024, **288**, 119827.

S10. F. Li, D. Wang, Q. Xing, G. Zhou, S. Liu, Y. Li, L. Zheng, P. Ye and J. Zou, *Appl. Catal. B: Environ.*, 2019, **243**, 621-628.